J Solid State Electrochem (2007) 11: 84–89
DOI 10.1007/s10008-005-0073-z

ORIGINAL PAPER

Andrea Kellenberger · Nicolae Vaszilcsin · Waltraut Brandl

Roughness factor evaluation of thermal arc sprayed skeleton nickel electrodes

Received: 6 June 2005 / Revised: 29 July 2005 / Accepted: 6 September 2005 / Published online: 4 November 2005

Abstract Skeleton nickel electrodes obtained by thermal arc spraying technique were characterized by different methods including scanning electron microscopy, energy dispersive X-ray analysis, X-ray diffraction, and electrochemical impedance spectroscopy. The skeleton electrodes reveal a highly porous structure with a surface roughness of about 270, determined from double layer capacitances obtained from impedance spectra.

Keywords Roughness factor · Electrochemical impedance spectroscopy · Skeleton nickel electrode

Introduction

A large number of electrochemical reactions, including hydrogen evolution/oxidation reactions (HER/HOR) and oxygen reduction reactions (ORR), as well as some organic compound reduction reactions, are catalyzed by platinum group metals. The electrochemical research in this field is focused on the reduction of the noble metal loading of the electrocatalyst, or its complete replacement with other, less expensive, materials that have similar electrocatalytic properties. One of the intensively studied metals, which fulfills both economic and electrocatalytic requirements, is nickel. The following methods are usually applied to enhance the electrocatalytic activity of nickel: the increase of the metal's real surface area, and the increase of the metal's intrinsic activity by doping it with transitional metals.

The increase of the real surface area may be achieved by depositing nickel together with an active metal like Al or Zn (i.e. by pressing [1–3], electrodeposition [4–6], composite coating [7–9], and thermal spray [10–13]) followed by the dissolution of the secondary component. As a result, a porous, three-dimensional structure is obtained, characterized by a high surface roughness factor.

Evaluation of the roughness factor, R, is possible by ex situ and in situ methods. In situ determinations are suitable for electrochemical studies because they give an estimate of the metal/electrolyte interface involved in the process. Various methods, which are based on the determination of an electrochemical property related to the surface area, have been proposed. For nickel electrodes the roughness factor is determined either from double layer capacitances using electrochemical impedance spectroscopy (EIS) [14–18], from the charge of nickel oxidation using cyclic voltammetry [19–22] or chronopotentiometry [23, 24], or from the comparison of HER currents at a constant overpotential [24].

The aim of the present work is to determine the roughness factor of nickel-based electrodes from the values of double layer capacitance obtained from electrochemical impedance measurements. The electrodes used in this study were prepared by thermal arc spray deposition of nickel and aluminum wires; thus providing high aluminum content in the coating which is further removed by alkaline leaching to increase the real surface of the electrodes.

Experimental

Electrode preparation

The skeleton nickel electrodes were prepared by thermal arc spray technique, using G 30/4 SF-LD/U2 metal spray equipment from OSU Maschinenbau GmbH, Germany. For the deposition process two different wires were used, one of Ni (97% Ni, 3% Ti) acting as anode and one of Al

A. Kellenberger (✉) · N. Vaszilcsin
Faculty of Industrial Chemistry
and Environmental Engineering,
University "Politehnica" of Timisoara,
Piata Victoriei nr. 2,
300006 Timisoara, Romania
e-mail: andreakellenberger@yahoo.com
Tel.: +40-256-404177
Fax: +40-256-403060

W. Brandl
Material Science Department,
University of Applied Sciences Gelsenkirchen,
Neidenburger Str. 10,
45877 Gelsenkirchen, Germany

(99.5% Al) acting as cathode. During the thermal spray the arc current and voltage were set to 160 A and 44 V, respectively. The spraying distance was maintained between 50 and 70 mm, and the atomizing gas (air) pressure was 1.7 bars. After the deposition the coating had a thickness of about 1 mm.

A carbon steel plate with dimensions of 100×300×3 mm was used as a support for the nickel–aluminum coating. Prior to the deposition the substrate was de-greased and sanded with corundum in order to assure an adequate adherence.

Investigations were carried out on samples cut out from the coated steel plates with diameters of 15 mm. To achieve an increase in the specific surface area of the electrodes, the samples were submitted to alkaline leaching in a 1 M NaOH solution at 80°C, for 2 h. After the dissolution of Al the samples were cleaned for 10 min in an ultrasound bath. From this point on, they will be referred to as skeleton electrodes.

Electrode characterization

The morphology of the electrodes was studied by scanning electron microscopy (SEM) with a Philips XL 30 ESEM microscope, working at 20 kV and at different magnitudes. The cross-section images were further analysed with an image processing software to determine porosity. For this purpose ImageJ, which is a public domain software written by W.S. Rasband [25], was used. The composition of the samples before and after leaching was determined by Energy Dispersive X-ray analysis coupled with SEM. X-ray diffraction patterns were registered with a Philips X'Pert Diffractometer, with Cu-Kα radiation (λ=1.54184 Å).

Electrochemical measurements

The electrochemical measurements were performed in a conventional three electrode Pyrex cell. The working electrode was composed of skeleton nickel embedded in a Teflon holder, exposing a geometric surface area of 1 cm^2. A Luggin capillary was placed approximately 1 mm from the electrode surface to minimise the *iR* drop. The counter-electrodes were two graphite roads and the reference—a saturated calomel electrode. Impedance spectra were recorded in the frequency range from 3 kHz to 10 mHz using a frequency response analyser based on an AT-MIO 16F5 National Instruments data acquisition board connected to an analogue PS3 Potentiostat. Measurements were conducted in potentiostatic mode at three different potentials (−1.1, −1.15 and −1.2 V vs SCE) corresponding to moderate HER over-potentials (−45, −95 and −145 mV). All determinations were made in 1 M of NaOH (Merck, pa) solution at 25°C.

The experimental data were fitted to the equivalent electrical circuits by a complex non-linear least squares (CNLS) Levenberg–Marquardt procedure using the ZView-Scribner Associates Inc. software.

Results and discussion

Morphology and composition of the skeleton Ni-electrodes

Figure 1 shows the SEM micrographs of the skeleton nickel electrode for the surface and cross-section, before and after aluminum dissolution.

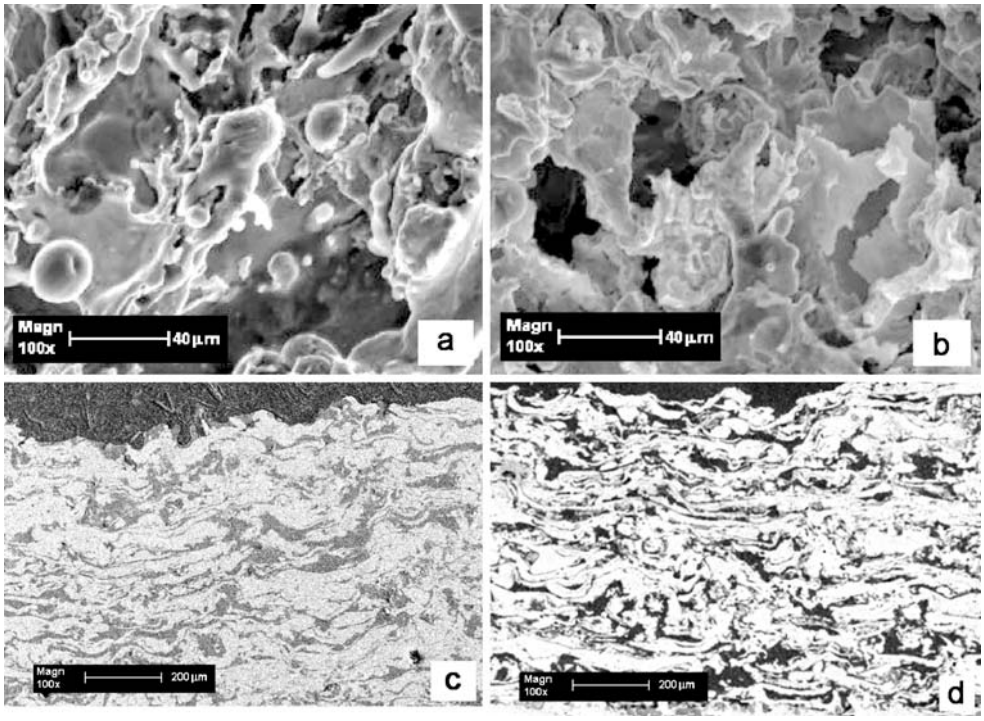

Fig. 1 SEM images of the nickel–aluminum coating. **a** As sprayed-surface; **b** after 120 min leaching-surface; **c** as sprayed-cross section; **d** after 120 min leaching-cross section

Table 1 Coating analysis

Treatment	Al		Ni		Ti		Fe		Porosity (%)
	wt.%	vol%	wt.%	vol%	wt.%	vol%	wt.%	vol%	
Before leaching	22.2	46.8	69.2	44.3	5.0	6.3	3.6	2.6	≈5[a]
After leaching	2.8	8.2	87.3	77.1	6.4	11.2	3.5	3.5	38.2

[a] approximate value for thermal arc sprayed coatings

Before leaching a typical structure for thermal arc spray is observed, characterized by the interconnection, deformation and flattening of the molten droplets. The particles' dimensions vary greatly due to asymmetrical melting [26] of the anode and cathode during thermal arc spray. The anode (nickel wire) melts slowly resulting in relatively large, elongated droplets, while the cathode (aluminum wire) melts quickly forming small, spherical droplets. The melting of the cathode has been found to contribute to the increase in porosity. The structure of the deposit after leaching shows a complete disappearance of the spherical shapes and the formation of holes in the structure of the coating.

The cross section micrographs of the coating reveal a lamellar, layered structure. The dark grey phase in Fig. 1c corresponds to aluminum and the brighter phase is related to nickel. After leaching it seems that the aluminum was completely removed from the coating. Also, it is noteworthy that the coating has preserved its integrity during Al dissolution, contrary to the shrinkage observed in the case of Raney nickel coatings. The thickness of the coating measured after Al dissolution was 0.8–0.9 mm.

The elemental composition of the coating was determined by energy dispersive X-ray (EDX) analysis. The porosity after leaching was evaluated from the cross section SEM images using ImageJ analyzing software. The obtained values are listed in Table 1. The presence of iron is related to the carbon steel substrate.

The aluminum content of the sample has a relatively high value before leaching and decreases by almost tenfold after dissolution. However, a small amount of aluminum still remains in the coating and is probably related to the presence of NiAl phase, which is resistant to alkaline leaching. The volume percent of each element was calculated from the weight percent value, taking into account the mass density of the respective element. When analyzing these values it is to be expected that the complete dissolution of aluminum should result in a porosity of 46.8%. However, aluminum is not entirely removed during the alkaline treatment; therefore, the porosity calculated as the difference between Al percent before and after leaching is only 38.6%. This value is in good agreement with the porosity obtained with ImageJ processing software (38.2%).

During thermal spray the residence time of the molten droplets in the hot gas stream is about one tenth of a second; therefore, it seems that there is a low probability for the formation of intermetallic compounds. However, if sufficiently high temperatures [27] or coating thickness [28] is provided during the coating growth, individual droplets may react, forming intermetallic compounds. Fig. 2 shows the X-ray diffraction patterns of the thermal-arc sprayed coating before and after leaching.

The X-ray diffraction pattern before leaching shows the appearance of well-defined, individual peaks, which is characteristic for metallic nickel and aluminum, but it also shows the presence of some ill-defined peaks (at 2θ=31.16;

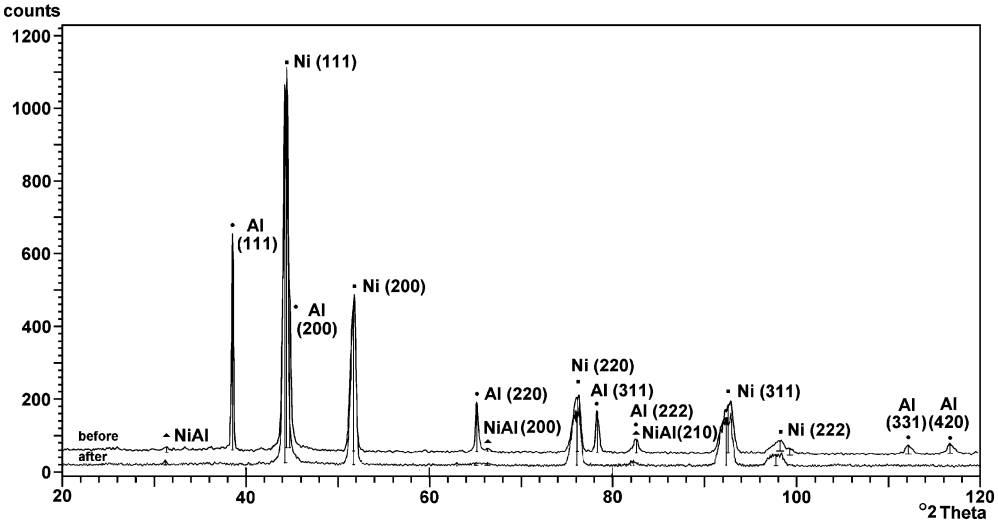

Fig. 2 X-ray diffraction pattern of the nickel–aluminum coating, before and after leaching

65.03; 82.06) attributed to the NiAl phase. The complete disappearance of the patterns associated to free aluminum is observed after leaching, concomitantly with the remanence of peaks characteristic of NiAl phase, which is resistant to alkaline leaching.

Impedance spectroscopy

The impedance spectra of the hydrogen evolution reaction on porous electrodes were often interpreted in terms of an equivalent electric circuit consisting of a parallel connection between the double layer capacitance C_{dl} and the faradaic impedance of the HER, Z_F, connected in series with the uncompensated solution resistance R_S. In this case the faradaic impedance is given by:

$$\frac{1}{Z_F} = A + \frac{B}{j\omega + C} \tag{1}$$

where A, B and C are parameters related to the rates of Volmer, Heyrovsky and Tafel steps of the HER mechanism [4, 7–9, 12, 16, 29] and ω is the angular frequency expressed in radians.

Another approach was developed by Armstrong and Henderson [30] who expressed the faradaic impedance of the HER as a combination of the charge transfer resistance R_{ct}, in series with a parallel connection between R_P and C_P. R_P is a pseudo-resistance related to the mass transfer resistance of the adsorbed intermediate (H_{ads}) and C_P is a pseudo-capacitance as it appears not from the electric double layer but from the faradaic reaction. The faradaic impedance is expressed by:

$$Z_F = R_{ct} + \left(R_P^{-1} + j\omega C_P\right)^{-1} \tag{2}$$

The parameters R_{ct}, R_P and C_P from the Armstrong's circuit are correlated to those from the first model by the following relations [7–9, 29]:

$$R_{ct} = \frac{1}{A} \tag{3}$$

$$R_P = -\frac{B}{A(AC + B)} \tag{4}$$

$$C_P = -\frac{A^2}{B} \tag{5}$$

In many cases the double layer capacitance from both models was approximated by a constant phase element (CPE) [1, 2, 4, 7–9, 12, 13] to explain the results obtained on solid electrodes that deviate from purely capacitive behavior and exhibit a frequency-dependent distribution of the double layer capacitance (Fig. 3a and b). Brug et al. assumed that this behavior is related to surface in-homogeneity and used Eq. 6 to describe the impedance of the constant phase element [31]:

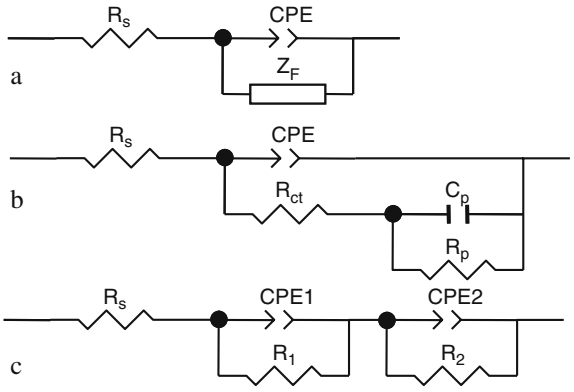

Fig. 3 Equivalent circuits used for the HER. **a** General model; **b** 1 CPE model; **c** 2 CPE model

$$Z_{CPE} = \frac{1}{T(j\omega)^{\phi}} \tag{6}$$

where T is a parameter related to the double layer capacitance according to relation 7 and ϕ is parameter between 0 and 1 describing the constant phase angle of the CPE.

$$T = C_{dl}^{\phi}\left(R_S^{-1} + R_{\infty}^{-1}\right)^{1-\phi} \tag{7}$$

To evaluate the surface roughness of the skeleton electrodes, double layer capacitances were determined by electrochemical impedance spectroscopy. Fig. 4 presents Nyquist and Bode plots obtained at three different electrode potentials situated in the hydrogen evolution region. The complex plane plots in Fig. 4a indicate the appearance of two depressed and overlapped semicircles at lower over-potentials (−45 and −95 mV), with the high frequency semicircle dependent on electrode potential. At higher over-potential (−145 mV) the experimental points are quite dispersed due to the intensification of hydrogen evolution, and only one deformed semicircle appears. Similar behavior has been reported by Choquette et al. [7, 8] and Okido et al. [9] for Raney nickel composite coated electrodes. Miousse et al. [12] also observed a potential-dependent behavior of the high frequency semicircle at reduced HER over-potentials for Ni-Al electrodes prepared by low pressure plasma spray.

The experimental data were fitted to the electrical model presented in Fig. 3b. Table 2 shows the obtained values of the circuit elements. In case of high over-potential, since only one semicircle is present, the parameters R_P and C_P could not be determined, and the impedance spectrum was fitted to a simplified model. This model contained a parallel connection between the charge transfer resistance and the

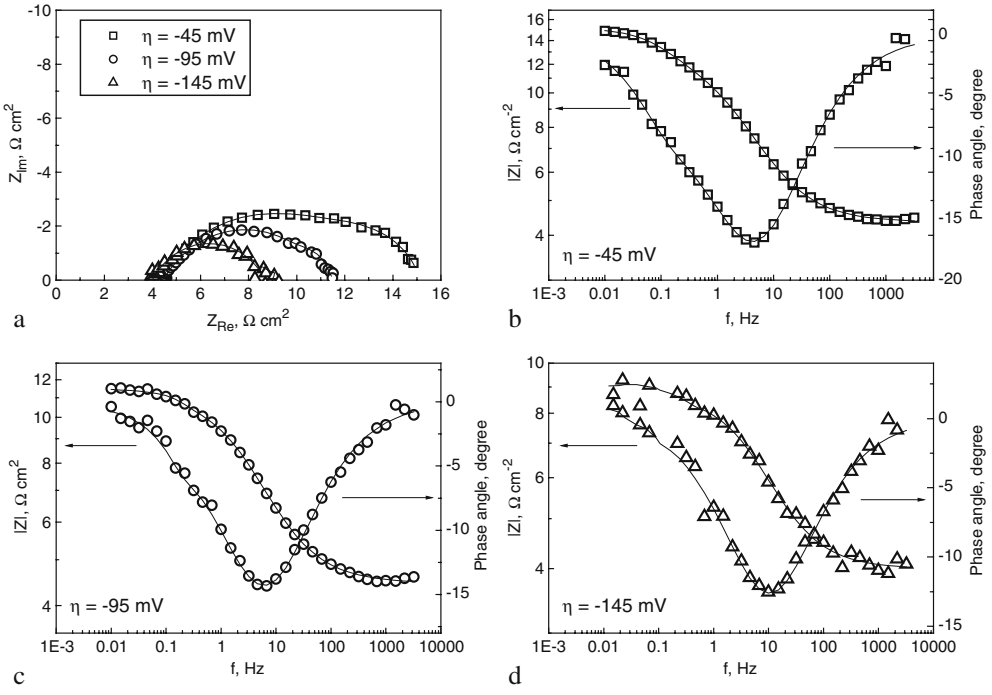

Fig. 4 Complex plane and Bode plots on skeleton nickel electrodes in 1 M NaOH solution at 25°C. *Open symbols* are experimental points and *continuous lines* are simulated by CNLS fitting according to the 1 CPE model

constant phase element in series with the solution resistance [2–4, 18, 23, 24, 32]. The total impedance of this model is given by:

$$Z = R_S + \left(R_{ct}^{-1} + T(j\omega)^{\phi}\right)^{-1} \quad (8)$$

The constant phase angle parameter ϕ is potential independent and has a value of approximately 0.65, close to the value of 0.5 which was predicted theoretically for porous electrodes [33]. Double layer capacitances calculated according to Eq. 7 are also presented in Table 2. The fact that the double layer capacity decreases with the increase of the electrode potential is ascribed to the occlusion of pores by gas bubbles due to the intensification of the hydrogen evolution reaction. Assuming a value of 20 μF cm^{-2} [1, 2, 4, 14, 24] suggested in the literature for the double layer capacity of a smooth nickel electrode, a surface roughness between 270 and 194 can be obtained depending on the electrode potential. The values of R decrease by 28% when increasing potential. This indicates that a fraction of the inner surface of the electrode is blocked during HER due to gas bubbles shielding.

The relatively low values of R are comparable to those reported for porous nickel electrodes obtained by galvanic deposition [34], as well as those reported for Ni-Zn electrodeposited [4] and Ni-Zn pressed powder [1] electrodes. Values as high as 45,000 were reported for plasma-sprayed Ni-Al electrodes [12], but in this case the substrate—a nickel grid—also contributed to the increase of the real surface area.

EIS studies conducted on thermal arc sprayed Ni-Al electrodes gave values of C_{dl} between 82 and 500 mF cm^{-2}, depending on the spray parameters such as the spraying distance and the angle between the gun and substrate [13]. Given these values, one may calculate the surface roughness, which ranges from 4,100 to 25,000. The impedance spectra in this case were fitted to the two-CPE (2 CPE) model introduced by Chen and Lasia [1] and Miousse et al. [12] containing two parallel R-CPE connections. This model predicts the formation of two semicircles on the complex plane plot, the first one connected with the po-

Table 2 Impedance data obtained from the 1 CPE model (Fig. 3b) in 1 M NaOH at 25°C

Parameter	η=−45 mV	η=−95 mV	η=−145 mV
R_S [Ω cm^2]	4.34±0.02	4.46±0.01	3.97±0.05
R_{ct} [Ω cm^2]	9.16±0.19	6.59±0.13	4.91±0.11
R_P [Ω cm^2]	1.67±0.16	0.51±0.11	–
C_P [F cm^{-2}]	0.697±0.119	1.127±0.440	–
T	0.0252±0.0009	0.0217±0.0009	0.0219±0.0020
ϕ	0.63±0.01	0.65±0.01	0.64±0.02
χ^2	$7.96\cdot10^{-4}$	$7.08\cdot10^{-4}$	$10.3\cdot10^{-4}$
C_{dl} [F cm^{-2}]	$5.41\cdot10^{-3}$	$4.74\cdot10^{-3}$	$3.88\cdot10^{-3}$
R	270	237	194

Table 3 Impedance data obtained from the 2 CPE model (Fig. 3c) in 1 M NaOH at 25°C

Parameter	η=−45 mV	η=−95 mV
R_S [Ω cm^2]	4.35±0.02	4.47±0.01
R_1 [Ω cm^2]	7.93±0.64	5.71±0.06
T_1	0.0237±0.0011	0.0210±0.0011
ϕ_1	0.64±0.01	0.66±0.01
R_2 [Ω cm^2]	2.91±0.69	1.39±0.03
T_2	0.45±0.18	0.38±0.04
ϕ_2	0.81±0.08	0.74±0.06
χ^2	$7.74\cdot10^{-4}$	$7.68\cdot10^{-4}$

rosity of the electrode and the second one related to the faradaic process.

Attempts have been made to fit our impedance data to the 2 CPE model presented in Fig. 3c. The results are given in Table 3.

The standard errors of the parameters determined with the 2 CPE model are, to some extent, higher than those obtained with the model containing one CPE, especially for the low frequency semicircle, while the goodness of fit (expressed by the Chi-squared value) remains almost unchanged. The inclusion of additional circuit elements in a model is justified by a tenfold decrease of the Chi-squared value; therefore, our impedance spectra are best fitted by the one-CPE (1 CPE) model rather than by the 2 CPE model. Moreover, the 2 CPE model was applied in cases where the high frequency semicircle could be related to the electrode porosity.

The dependence of the semicircle radius as a function of over-potential gives information as to whether it should be related to electrode porosity or to HER kinetics, since only the HER mechanism depends upon over-potential [16, 29]. Although only three over-potentials were considered in our study, a decreasing tendency of the radius of the high frequency semicircles is observed at increasing over-potentials, suggesting that it is more likely connected to the kinetics of the hydrogen evolution reaction than it is to porosity.

Conclusions

The results of the present study show that thermal arc spraying is a suitable technique to obtain high surface area nickel electrodes by deposition of a nickel wire together with an aluminum wire, followed by the alkaline dissolution of the aluminum. The SEM and EDX investigations reveal a noticeable increase in the electrode porosity associated with the decrease of the aluminum content from 22.2 to 2.8 wt.% during leaching. As determined by image analysis, the porosity of the skeleton nickel electrodes was almost 40%. X-ray diffraction indicates that only a small amount of un-leacheable NiAl phase is formed during thermal arc spray, consistent with the small percentage of aluminum found by EDX analysis after leaching.

The EIS measurements conducted on the skeleton nickel electrodes indicated the presence of two potential-dependent semicircles at reduced HER over-potentials, and only one semicircle at higher potential. Two electrical circuits (1 CPE and 2 CPE) were assumed to model the impedance data. Based on statistical analysis and on the kinetic nature of both semicircles it was found that the 1 CPE model describes more accurately our experimental results.

The roughness factor of the skeleton nickel electrodes estimated from double layer capacitance ranges between 270 and 194, depending on the electrode potential; and therefore, expresses the real electrochemical surface involved in the hydrogen evolution reaction, also accounting for surface modification due to gas bubbles shielding.

The values of R are in good agreement with those reported by us in an earlier study [35], in which the roughness factor was determined by cyclic voltammetry from the charge associated with the oxidation of the nickel electrode surface to a mono-layer of nickel hydroxide. This method gave values of R between approximately 260 and 450, depending on the working conditions of the thermal arc spraying process.

References

1. Chen L, Lasia A (1992) J Electrochem Soc 139:3214
2. Los P, Rami A, Lasia A (1993) J Appl Electrochem 23:135
3. Tanaka S, Hirose N, Tanaki T, Ogata YH (2001) Int J Hydrogen Energ 26:47
4. Chen L, Lasia A (1991) J Electrochem Soc 138:3321
5. de Giz MJ, Bento SC, Gonzalez ER (2000) Int J Hydrogen Energ 25:621
6. Sheela G, Pushpavanam M, Pushpavanam S (2002) Int J Hydrogen Energ 27:627
7. Choquette Y, Brossard L, Lasia A, Menard H (1990) J Electrochem Soc 137:1723
8. Choquette Y, Brossard L, Lasia A, Menard H (1991) Electrochim Acta 35:1251
9. Okido M, Depo JK, Capuano GA (1993) J Electrochem Soc 140:127
10. Schiller G, Borck V (1992) Int J Hydrogen Energ 17:261
11. Schiller G, Henne R, Borck V (1995) J Therm Spray Techn 4:185
12. Miousse D, Lasia A, Borck V (1995) J Appl Electrochem 25:592
13. Fournier J, Miousse D, Legoux JG (1999) Int J Hydrogen Energ 24:519
14. Miao HJ, Piron DL (1993) Electrochim Acta 38:1079
15. Simpraga RP, Conway BE (1998) Electrochim Acta 43:3045
16. Hitz C, Lasia A (2001) J Electroanal Chem 500:213
17. Tanaka S, Hirose N, Tanaki T (2000) Int J Hydrogen Energ 25:481
18. Tanaka S, Hirose N, Tanaki T, Ogata Y (2000) J Electrochem Soc 147:2242
19. de Giz MJ, Silva JPC, Ferreira M, Machado SAS, Ticianelli EA, Avaca LA, Gonzalez ER (1992) Int J Hydrogen Energ 17:725
20. de Giz MJ, Machado SAS, Avaca LA, Gonzalez ER (1992) J Appl Electrochem 22:973
21. Brown IJ, Sotiropoulos S (2000) J Appl Electrochem 30:107
22. Brown IJ, Sotiropoulos S (2001) Electrochim Acta 46:2711
23. Rausch S, Wendt H (1996) J Electrochem Soc 143:2852
24. Karimi Shervedani R, Lasia A (1999) J Appl Electrochem 29:979
25. Rasband WS (1997–2005) ImageJ, U. S. National Institutes of Health, Bethesda, Maryland, USA, http://rsb.info.nih.gov/ij/
26. Hussary NA, Heberlein JVR (2001) J Therm Spray Techn 10:604
27. Deevi SC, Sikka VK, Swindeman CJ, Seals RD (1997) J Therm Spray Techn 6:335
28. Newbery AP, Cantor B, Jordan RM, Singer ARE (1992) Scr Metall Mater 27:915
29. Birry L, Lasia A (2004) J Appl Electrochem 32:1
30. Armstrong RD, Henderson M (1972) J Electroanal Chem Interfacial Electrochem 39:81
31. Brug GJ, Van Der Eeden ALG, Sluyters-Rehbach M, Sluyters JH (1984) J Electroanal Chem 176:275
32. Panek J, Serek A, Budniok A, Rowinski E, Lagiewka E (2003) Int J Hydrogen Energ 28:169
33. De Levie R (1967) In: Delahay P (ed) Advances in Electrochemistry and Electrochemical Engineering, vol 6. Wiley, New York, p329
34. Huet F, Musiani M, Nogueira RP (2004) J Solid State Electr 8:786
35. Kellenberger A, Vaszilcsin N (2005) Rev Roum Chim 7:712